A three-gene signature correlated with MAPK/ERK activation characterizes acquired resistance to EGFR-tyrosine kinase inhibitors in non-small cell lung cancer

CHANGTAI QIN[1*], WEI ZHANG[2*], DONGFANG TANG[3*], YUXI YANG[1], BINGHUI LIANG[1], ZHIMING HU[4], YUXIAO ZHANG[5], TINGJIE YE[1] and WEI XU[1]

[1]School of Integrative Medicine, Shanghai University of Traditional Chinese Medicine, Shanghai 201203, P.R. China; [2]Department of Clinical Laboratory, Peking University Shenzhen Hospital, Shenzhen, Guangdong 518036, P.R. China; [3]Department of Thoracic Surgery, Huadong Hospital Affiliated to Fudan University, Shanghai 200040, P.R. China; [4]Department of Pharmacology, School of Medicine, University of California, San Diego, CA 92093, USA; [5]Department of Oncology and Institute of Traditional Chinese Medicine in Oncology, Longhua Hospital, Shanghai University of Traditional Chinese Medicine, Shanghai 200032, P.R. China

Received August 21, 2025; Accepted June 12, 2026

DOI: 10.3892/ol.2026.15768

Abstract. Epidermal growth factor receptor-targeted therapies such as afatinib provide clinical benefits to patients with advanced-stage non-small cell lung cancer (NSCLC); however, acquired resistance frequently develops, with the underlying mechanisms remaining undefined in 20-30% of cases. The present study established afatinib-resistant (AR) NSCLC cell lines and confirmed their resistance phenotype using Cell Counting Kit-8 (CCK-8) cell viability assays. Notably, these cells also exhibited cross-resistance to osimertinib. To elucidate the molecular basis of resistance acquisition, the time-resolved transcriptomic profiling of A549 cells was performed across three stages: Parental, afatinib-exposed (adaptive phase) and stable resistant cells. The analyzed results revealed the persistent upregulation of *ABLIM3*, *HTR1D* and *HSPA1A*, which was validated by reverse transcription-quantitative polymerase chain reaction. The meta-analysis of hazard ratios from The Cancer Genome Atlas demonstrated that the elevated expression level of the three-gene signature was significantly associated with tumor progression and an increased risk of disease recurrence. These transcriptional alterations were accompanied by the sustained activation of the MAPK/ERK signaling pathway, as evidenced by increased ERK1/2 phosphorylation detected using western blot analysis, which was positively associated with the expression level of the three-gene signature. Functional analyses further demonstrated that the pharmacological inhibition of MAPK/ERK signaling using selumetinib effectively re-sensitized AR cells to both afatinib and osimertinib, as demonstrated by restored drug sensitivity in CCK-8 assays. Collectively, these findings suggest that MAPK/ERK signaling contributes to the transition from adaptive tolerance to stable resistance to afatinib and highlight a tractable therapeutic vulnerability for overcoming resistance to tyrosine kinase inhibitors in NSCLC.

Correspondence to: Professor Wei Xu or Professor Tingjie Ye, School of Integrative Medicine, Shanghai University of Traditional Chinese Medicine, 1200 Cailun Road, Shanghai 201203, P.R. China
E-mail: wei-xu11@tsinghua.org.cn
E-mail: yetj81@163.com

*Contributed equally

Key words: non-small cell lung cancer, tyrosine kinase inhibitor resistance, adaptive response, ERK1/2, afatinib, osimertinib

Introduction

According to global cancer statistics data reported in 2024, lung cancer remains the leading cause of cancer-related mortality, accounting for 20% of all cancer-related mortalities worldwide (1). Lung cancer is classified into small cell lung cancer and non-small cell lung cancer (NSCLC) based on histopathological characteristics, with NSCLC accounting for 80% of lung cancer cases (2). Clinical statistics indicate that ≥70% of patients with NSCLC are diagnosed at an advanced stage (3), with the 5-year survival rate for patients with advanced NSCLC being <10% (4). The 2022 NCCN Clinical Practice Guidelines for NSCLC recommend targeted therapy as the preferred first-line treatment for advanced-stage NSCLC (5).

Epidermal growth factor receptor (EGFR) is a member of the erythroblastic leukemia viral oncogene B (ErbB) family. Upon ligand binding, the activated tyrosine kinase domain of EGFR triggers downstream signaling pathways, which subsequently promote tumor cell proliferation, differentiation and migration (6). Abnormally high EGFR expression is present in >60% of NSCLC tumor tissues (7). As a result, EGFR has become a key target for targeted therapy in advanced-stage NSCLC. Tyrosine kinase inhibitors (TKIs) have been developed and extensively applied in the treatment of advanced-stage NSCLC

with EGFR activation (8). Among the EGFR-targeting TKIs, second-generation inhibitors are increasingly recognized for their pan-ErbB inhibitory activity, rendering them particularly effective in the treatment of uncommon EGFR mutations (9). Afatinib, as an irreversible inhibitor of the ErbB family, has demonstrated robust preclinical inhibitory activity against both wild-type and mutant EGFR (10). However, afatinib treatment leads to acquired resistance, leading to clinical treatment failure (11). Therefore, elucidating the molecular mechanisms underlying resistance to afatinib is key to addressing the clinical challenge of resistance to afatinib.

Numerous studies have revealed EGFR secondary mutations (12), oncogene amplification (13) and cellular phenotypic transitions (14), which contribute to the resistance to afatinib in NSCLC. However, 20-30% of drug-resistant cases remain to be elucidated, suggesting the involvement of unidentified mechanisms (15,16). Notably, tumors often undergo various adaptive responses during cancer treatment, which are key contributors to treatment failure and the development of resistance. Resistance caused by an adaptive response is a non-cell-autonomous mechanism by which tumor cells acquire transient drug resistance through the rapid reprogramming of signaling pathways, metabolism or phenotypic plasticity, without the genetic or epigenetic alterations (17,18). While this resistance may be reversed upon the cessation of the drug, it can also lay the groundwork for the subsequent development of stable resistance (19,20). Due to the dual role of short-term adaptive responses in the resistance to afatinib, longitudinal transcriptome profiling was conducted in the present study using A549 parental cells, afatinib-treated A549 cells, and afatinib-resistant A549-AR cells to identify resistance signatures and underlying signaling pathways throughout resistance development.

The aim of the present study was not to re-evaluate the canonical EGFR-targeted efficacy of afatinib, but to elucidate the cellular stress responses elicited by TKI exposure in NSCLC cells. Specifically, the present study investigated the mechanisms through which drug-induced adaptive responses, characterized by cytokine secretion, signaling reprogramming and stress-related protein upregulation, contribute to the initiation of resistance. To minimize confounding from constitutively active EGFR mutations, EGFR-wild-type NSCLC cell lines (A549 and H1299) were employed, thereby enabling the exploration of EGFR-independent adaptive mechanisms underlying TKI-induced resistance. Using RNA-sequencing (RNA-seq) analysis on both short-term afatinib-treated and stably resistant cells, the present study further delineated the dynamic transcriptional changes that accompany the transition from adaptive tolerance to stable resistance.

Materials and methods

Cell lines and culture. The A549 and H1299 cell lines, obtained from the National Collection of Authenticated Cell Cultures, were maintained in RPMI-1640 medium supplemented with 10% fetal bovine serum (GeminiBio LLC). The cells were incubated at 37˚C in a humidified atmosphere with 5% CO_2. The mutation profiles of EGFR, Ras and p53 in all NSCLC cell lines were confirmed according to the Catalogue Of Somatic Mutations In Cancer and American Type Culture Collection databases (Table SI). All cell lines were authenticated using short tandem repeat profiling and were routinely evaluated for mycoplasma contamination.

Drug preparation. Afatinib, osimertinib, selumetinib and SB431542 were purchased from Selleck Chemicals and dissolved in 100% DMSO at stock concentrations of 10 mM. All these drugs were stored at -20˚C for long-term use.

Establishment of afatinib resistant cells. The A549 and H1299 cells were exposed to serial concentrations of afatinib (2, 5, 7.5, 10 and 12 μM) at 50% confluency for 3 days, with each concentration repeated for a minimum of two treatment cycles. Subsequently, the established afatinib-resistant (AR) cells (A549-AR and H1299-AR) were validated using the Cell Counting Kit-8 (CCK-8) assay. Briefly, parental and AR cells were treated with 1, 2, 5 and 10 μM afatinib for 48 h to validate afatinib resistance, and with 1, 2, 5 and 10 μM osimertinib for 48 h to assess cross-resistance.

CCK-8 assay. The cells were digested and resuspended to a concentration of $1x10^5$ cells/ml. A total of 30 μl of the resuspended cell suspension was added into 1 ml culture medium and subsequently seeded into 96-well plates. Following overnight incubation at 37˚C, the medium was replaced with fresh medium containing SB431542 or selumetinib at 1 or 10 μM, and the cells were incubated at 37˚C for an additional 48 h. Subsequently, 10 μl CCK-8 reagent (Selleck Chemicals) was added to each well and the plates were incubated for 2-4 h at 37˚C. The absorbance was measured at 450 nm using a microplate reader (Agilent Technologies, Inc.).

Reverse transcription-quantitative polymerase chain reaction (RT-qPCR). Total RNA was extracted from the A549 cells, A549 cells treated with 20 μM afatinib for 48 h and A549-AR cells using TRIzol® reagent (Thermo Fisher Scientific, Inc.) according to the manufacturer's protocol. First-strand complementary DNA (cDNA) was synthesized from 1 μg total RNA using the Hifair® III 1st Strand cDNA Synthesis SuperMix according to the manufacturer's protocol (Shanghai Yeasen Biotechnology Co., Ltd.). qPCR was performed using ChamQ Universal SYBR® qPCR Master Mix (Vazyme Biotech, Co., Ltd.) on a RT-PCR system (Roche Diagnostics). Each 20-μl reaction mixture contained 10 μl ChamQ SYBR® qPCR Master Mix, 0.4 μl of forward primer (10 μM), 0.4 μl of reverse primer (10 μM), 1 μl of cDNA template and 8.2 μl of nuclease-free water. The thermal cycling conditions were as follows: Initial denaturation at 95˚C for 30 sec, followed by 40 cycles of denaturation at 95˚C for 10 sec and annealing/extension at 60˚C for 30 sec. Relative gene expression was calculated using the $2^{-\Delta\Delta Cq}$ method (21), with GAPDH serving as the internal reference gene. The primer sequences were designed by author WX and are listed in Table SII.

Western blotting. The A549 and A549-AR cells were lysed in RIPA buffer (X-Blot Technology Co., Ltd.) containing protease and phosphatase inhibitors on ice for 30 min. Lysates were centrifuged at 12,000 x g for 15 min at 4˚C and the supernatants were collected. Protein concentrations were quantified

using a BCA protein assay kit (Thermo Fisher Scientific, Inc.) following the manufacturer's instructions. Equal amounts of protein (20 μg per sample) were resolved on 10% gels using SDS-PAGE and transferred to PVDF membranes (MilliporeSigma). The membranes were blocked with 5% bovine serum albumin in TBST (20 mM Tris-HCl, 150 mM NaCl, 0.1% Tween-20 and pH 7.5) for 1 h at room temperature and incubated overnight at 4˚C with primary antibodies against ERK1/2 (cat. no. 4695; 1:1,000; Cell Signaling Technology, Inc.), anti-phospho-ERK1/2 (Thr202/Tyr204; cat. no. 4370; 1:1,000; Cell Signaling Technology, Inc.) and GAPDH as the reference (cat. no.60004-1-Ig; Proteintech Group, Inc.). After washing with 1X TBST containing 0.1% Tween-20 (v/v), the membranes were incubated with HRP-conjugated anti-rabbit IgG secondary antibody [cat. no. BE0106; 1:5,000; Baioyijie (Beijing) Technology Co., Ltd.] or HRP-conjugated anti-mouse IgG secondary antibody [1:5,000; cat. no. BE0104; Baioyijie (Beijing) Technology Co., Ltd.] for 1 h at room temperature. Bands were visualized using an enhanced chemiluminescence kit (X-Blot Technology Co., Ltd.) and captured with the ChemiDoc XRS+ imaging system (Bio-Rad Laboratories, Inc.). Band intensities were quantified using ImageJ software (version 1.54; National Institutes of Health). The p-ERK/ERK ratio was calculated for quantitative analysis, and GAPDH was used as the loading control.

RNA-seq and differential gene analysis. RNA was extracted from A549 cells, A549 cells treated with 20 μM afatinib for 48 h and A549-AR cells using TRIzol reagent (Thermo Fisher Scientific, Inc.). The extracted RNA samples were submitted to Genewiz, Inc., for RNA sequencing as a commercial sequencing service, and subsequent RNA quality assessment, library preparation and sequencing were performed by the company. RNA quality and integrity were assessed using NanoDrop spectrophotometry (Thermo Fisher Scientific, Inc.) and RNA Quality Score analysis. Libraries were prepared using the VAHTS® Universal V8 RNA-seq Library Prep Kit for Illumina (cat. no. NR605; Vazyme Biotech Co., Ltd.). Paired-end sequencing with a read length of 150 bp (PE150) was performed (all other methods details are proprietary to Genewiz, Inc.). The RNA sequencing data were processed and analyzed in RStudio (version 2025.9.2.418; Posit Software), with differential gene expression calculated using the 'DESeq2' package (version 1.50.2; Bioconductor). The differential gene expression analysis was performed among the following comparisons: i) Treated A549 cells vs. A549 cells; ii) A549-AR cells vs. A549 cells; and iii) A549-AR cells vs. treated A549 cells. Gene Ontology (GO) enrichment analysis was performed for biological process, molecular function and cellular component categories (http://geneontology.org/). Kyoto Encyclopedia of Genes and Genomes (KEGG) pathway enrichment analysis was also performed (https://www.genome.jp/kegg/).

Time-series analysis. Time-series gene expression analysis was performed using the 'maSigPro' package (version 1.82.0; Bioconductor). Expression data were organized by time points and treatment conditions. Model fitting was performed using 'p.vector' with Q set to 0.05 and counts set to false, followed by backward stepwise regression using 'T.fit'. Significant genes were identified using 'get.siggenes', applying an R-squared threshold of 0.7 and selecting all condition variables. Genes with adjusted P-values <0.05 were retained for visualization and downstream functional analysis.

Survival analysis for genes. Overall survival (OS) and disease-free survival (DFS) analyses were performed using the Gene Expression Profiling Interactive Analysis 2 (GEPIA2) web tool (http://gepia2.cancer-pku.cn/#survival), which is based on data from The Cancer Genome Atlas (TCGA; https://portal.gdc.cancer.gov/) and the Genotype-Tissue Expression databases (GTEx; https://gtexportal.org/home/). Survival curves were generated based on gene expression levels, with the group cut-off set to the quartile method to define the low-expression group as patients in the lowest 25% of gene expression and the high-expression group as patients in the highest 25% of gene expression. Patients with gene expression levels in the middle 50% were not included. For Kaplan-Meier curves showing crossover, P-values were estimated using the two-stage procedure as previously described (22,23) and implemented in the TSHRC package (version 0.1-6; https://cran.r-project.org/package=TSHRC). As individual-level raw survival data and full analysis settings were not available from GEPIA, the two-stage analysis was performed on survival coordinates digitized from the Kaplan-Meier plots using WebPlotDigitizer (version 5.2; Automeris; https://automeris.io/WebPlotDigitizer/); therefore, the resulting two-stage P-values should be interpreted as approximate. Hazard ratios (HRs) shown in the GEPIA2 survival plots were used as summary effect estimates over the full follow-up period.

Correlation analysis. ERK signaling-related genes, including EGFR, KRAS, NRAS, HRAS, BRAF, Raf1, MAP2K1, MAP2K2, MAPK3, MAPK1, FOS, FOSL1, FOSL2, Jun, JunB, JunD, dual-specificity phosphatase (DUSP)6, EGR1, CCND1, SPRY2, ETV4 and ETV5, were selected and entered into the first gene signature input in GEPIA2. The three-gene resistance signature (*ABLIM3*, *HTR1D* and *HSPA1A*) was entered into the second gene signature input. Pearson's correlation analysis was subsequently performed using TCGA-lung adenocarcinoma tumor dataset.

Meta-analysis. The HRs were obtained from the GEPIA2 survival plots. The corresponding 95% confidence intervals (CIs) were calculated based on the reported HRs and P-values. Subsequently, the HRs and their 95% CIs for differentially expressed genes or cancer types were pooled to calculate the overall effect estimates, applying a random-effects model. An HR >1 with the lower bound of the 95% CIs >1 indicated that the high expression level of the gene was significantly associated with reduced survival. A meta-analysis was performed using STATA software (version 16.0; StataCorp LP; https://www.stata.com/).

Statistical analysis. Data are presented as the mean ± standard error of the mean from at least three independent replicates. All statistical analyses were performed using GraphPad Prism software (version 10.6.1; Dotmatics). Statistical comparisons between two groups were performed using

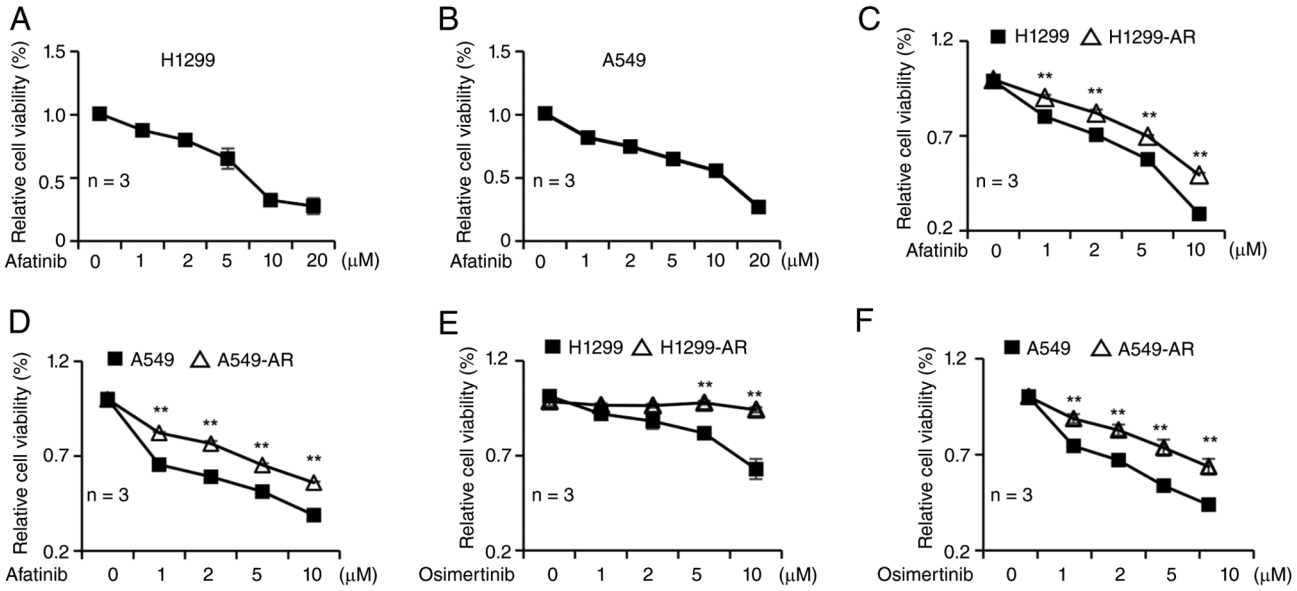

Figure 1. Cells with acquired resistance to afatinib exhibit cross resistance to tyrosine kinase inhibitors. (A and B) Relative cell viability of (A) H1299 and (B) A549 cells treated with serial concentrations of afatinib (n=3). (C) Relative cell viability of H1299 and H1299-AR cells treated with serial concentrations of afatinib (n=3). (D) Relative cell viability of A549 and A549-AR cells treated with serial concentrations of afatinib (n=3). (E) Relative cell viability of H1299 and H1299-AR cells treated with serial concentrations of osimertinib (n=3). (F) Relative cell viability of A549 and A549-AR cells treated with serial concentrations of osimertinib (n=3). **P<0.01, compared with parental cells. AR, afatinib-resistant.

unpaired two-tailed Student's t-tests. When multiple treatment groups were compared, homogeneity of variance was first evaluated using the Brown-Forsythe (or Levene's) test; if the equal-variance assumption was met, one-way ANOVA followed by Tukey's or Dunnett's multiple-comparisons test was used and the corresponding adjusted P-values were reported. Specifically, Dunnett's multiple-comparisons test was applied for many-to-one comparisons in which all groups were compared with a single pre-specified reference group, whereas Tukey's multiple-comparisons test was used for analyses involving multiple pairwise comparisons among groups. If variances were unequal, Welch's one-way ANOVA was applied; post hoc multiple comparisons were performed using the Games-Howell test. When data did not meet parametric assumptions, the Kruskal-Wallis's test followed by Dunn's multiple-comparisons test was used. P<0.05 was considered to indicate a statistically significant difference.

Results

Cells with acquired resistance exhibit cross resistance to TKIs. To investigate the molecular mechanisms underlying acquired resistance to afatinib, AR cell lines were established. Initially, the optimal concentration of afatinib was determined based on cytotoxic effects. A range of afatinib concentrations was administered to the H1299 and A549 cells, revealing that a dose of 2 μM reduced cell viability by 20% (Fig. 1A and B). Therefore, the induction of acquired resistance was initiated using 2 μM afatinib, as this concentration provided sufficient selective pressure while still allowing surviving cells to recover and gradually adapt during subsequent treatment cycles. The H1299-AR cells exhibited a significantly reduced sensitivity to afatinib, as evidenced by the significantly lower inhibition of cell viability compared with the parental H1299 cells under identical treatment conditions (P<0.01; Fig. 1C). A similar resistance phenotype was observed in the A549-AR cells (P<0.01; Fig. 1D). Furthermore, both the H1299-AR and A549-AR cells demonstrated cross-resistance to osimertinib treatment, as shown by significantly higher cell viability at 5 and 10 μM in H1299-AR cells and at 1, 2, 5 and 10 μM in A549-AR cells compared with their parental cells (Fig. 1E and F). These findings suggested that the acquired resistance in NSCLC cells is not limited to afatinib, but extends to third-generation EGFR-TKIs, such as osimertinib. This suggested that the underlying mechanism may be independent of the EGFR mutation status and instead may be associated with adaptive responses contributing to acquired resistance.

Transcriptome dynamics and functional enrichment reveal molecular transition from drug sensitivity to resistance. To investigate the adaptive responses driving the transition from drug sensitivity to stable acquired resistance, the transcriptome profiling of sensitive, treated and resistant cells was conducted (Fig. 2A). Hierarchical clustering analysis revealed distinct segregation among the three groups, with the treated cells exhibiting an intermediate transcriptional state, indicative of a stepwise progression toward resistance (Fig. 2B). Gene expression trajectories revealed a variety of dynamic patterns, such as high-low-high, high-high-low, low-high-high, low-high-low and low-low-high, emphasizing the heterogeneous nature of transcriptional reprogramming during resistance acquisition (Fig. 2C). The low-high-high pattern observed in cluster 3 was characterized by constitutively upregulated genes that potentially contribute to afatinib acquired resistance. To further investigate the functional significance of these persistently upregulated genes, GO analysis was conducted on cluster 3.

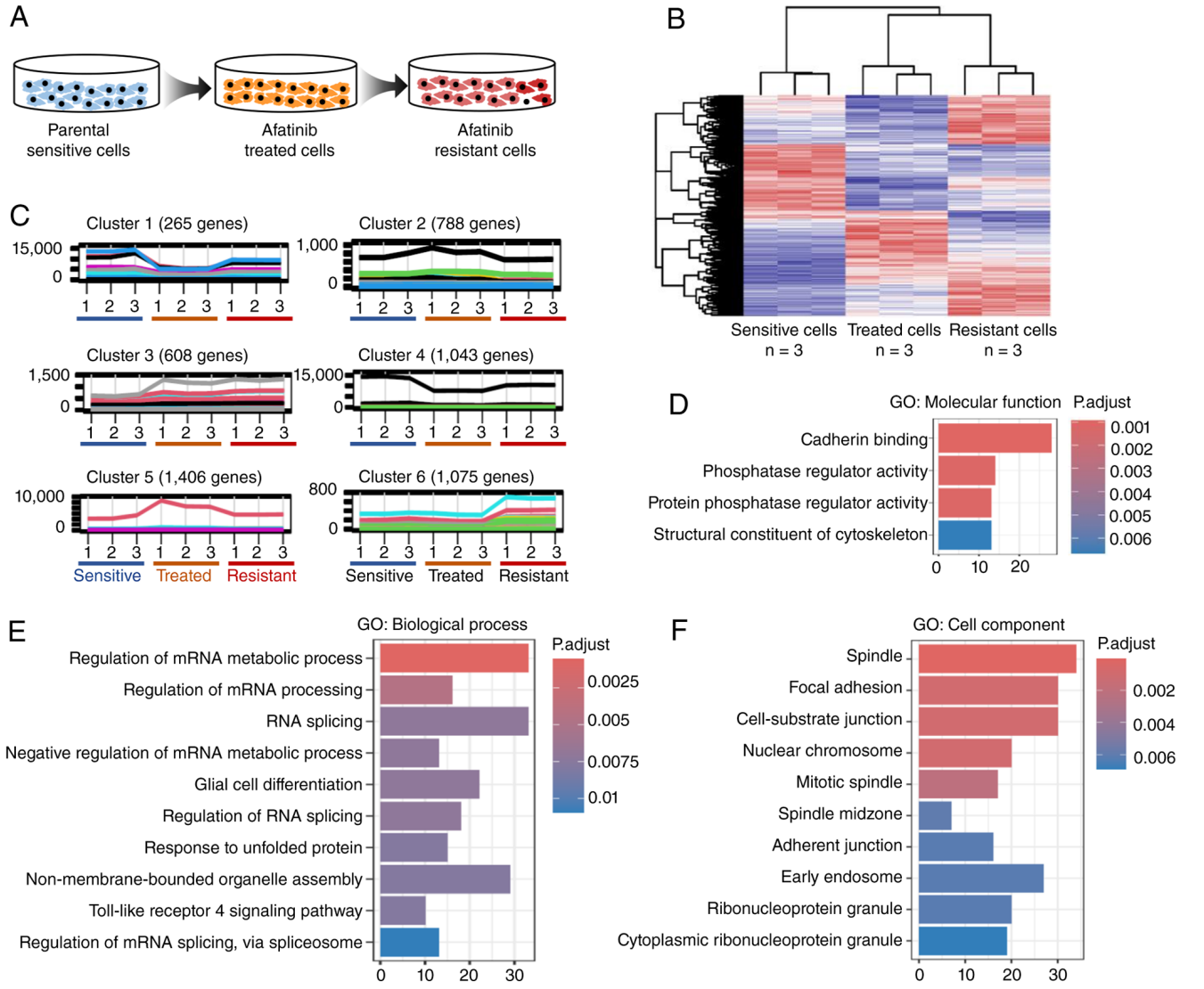

Figure 2. Transcriptome dynamics and functional enrichment reveal molecular transition from drug sensitivity to resistance. (A) Flowchart of RNA-sequencing analysis in A549 sensitive cells, A549 cells treated with afatinib for 48 h and A549-AR cells. (B) Heatmap of the significant genes after Time-series analysis of gene expression using 'maSigPro' package (n=3). (C) Time-course analysis of differential gene expression across sensitive, treated and resistant states. (D-F) GO (D) molecular function, (E) biological process and (F) cell component analysis for genes in cluster 3. GO, Gene Ontology; AR, afatinib resistant.

GO molecular function analysis revealed significant enrichment in 'cadherin binding', 'phosphatase regulator activity' and 'protein phosphatase regulator activity' ($P<0.05$; Fig. 2D), suggesting the enhanced regulation of kinase-phosphatase signaling and cell-cell adhesion, which may contribute to the resistant phenotype. GO biological process analysis identified pronounced enrichment in RNA-related functions, including 'regulation of mRNA metabolic process', 'regulation of mRNA processing' and 'RNA splicing' (Fig. 2E), implicating elevated transcriptional and post-transcriptional activity in the maintenance of resistance. Furthermore, cellular component analysis indicated significant enrichment in 'spindle', 'focal adhesion' and 'cell-substrate junction' ($P<0.05$; Fig. 2F), consistent with increased mitotic activity and dynamic cytoskeletal remodeling. These functional analyses suggested that resistance to afatinib is associated with enhanced kinase-phosphatase signaling, cell adhesion, and increased transcriptional and post-transcriptional activity.

Identification and characterization of differentially expressed genes during the transition from drug sensitivity to resistance. To identify the constitutively upregulated gene signature contributing to acquired resistance to afatinib, genes with a ≥2-fold increase in expression were selected in both treated and AR cells. As presented in the volcano plots, the treated cells displayed a moderate number of differentially expressed genes, while the resistant cells exhibited a more extensive transcriptional shift, reflecting a progressive reprogramming of gene expression (Fig. 3A). Venn diagram analysis further revealed that a subset of upregulated (n=63) and downregulated (n=219) genes was shared between the treated and resistant groups, while the majority were uniquely enriched in resistant cells (Fig. 3B), suggesting a gradual development toward a resistant state. Hierarchical clustering demonstrated clear segregation among the three groups, with treated cells occupying an intermediate transcriptional position, consistent with a gradual acquisition of resistance (Fig. 3C). Furthermore, representative gene trajectories revealed distinct

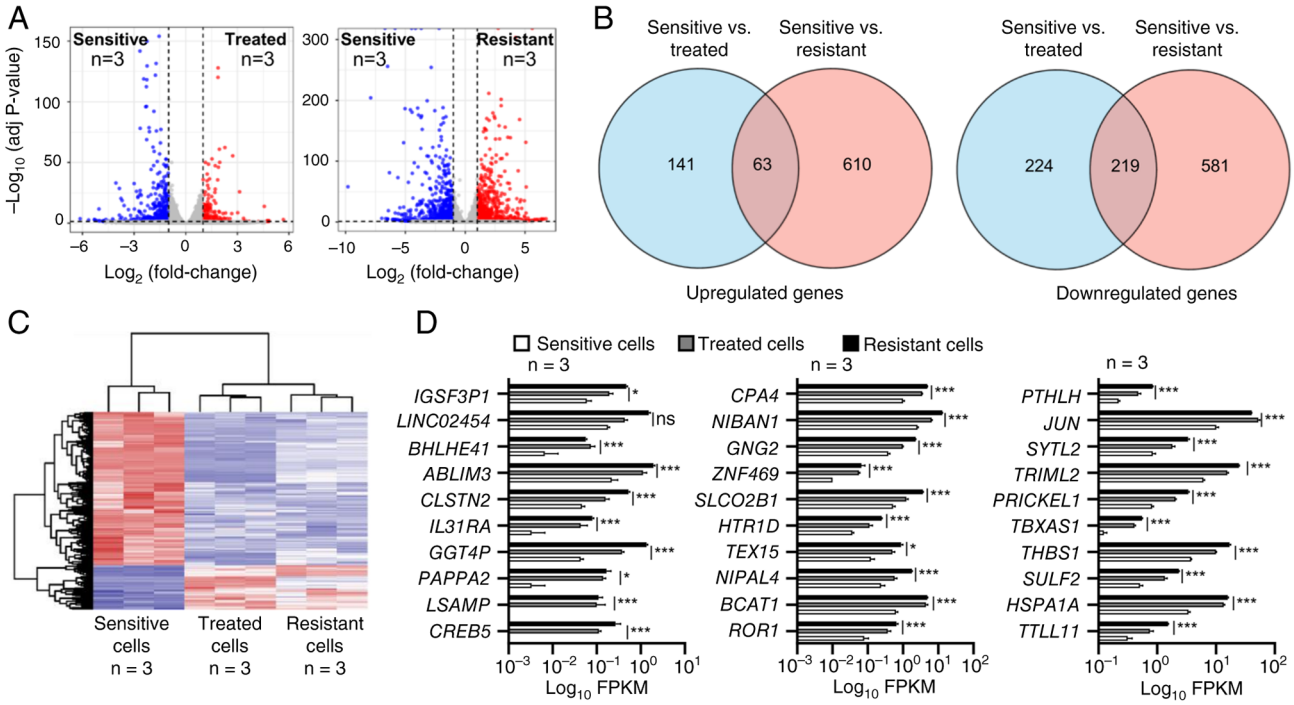

Figure 3. Identification and characterization of differentially expressed genes during the transition from drug sensitivity to resistance. (A) Volcano plot of the differential genes with 2-fold changes in treated and resistant cells compared with sensitive cells, n=3. (B) Overlapping of the upregulated and downregulated genes with 2-fold changes. (C) Heatmap images for the 63 continuously upregulated genes or 219 downregulated genes in the treated and resistant groups (n=3). (D) Comparison of the top 30 upregulated genes in treated or resistant cells versus sensitive cells (n=3). Statistical significance was assessed by one-way ANOVA followed by Dunnett's multiple-comparisons test versus the control; *P<0.05, ***P<0.001. ns, not significant; FPKM, fragments per kilobase of transcript per million mapped reads.

dynamic expression patterns, including persistent upregulation of resistance-associated genes such as *JUN*, *HSPA1A* and *SYTL2* (Fig. 3D), indicating a time-dependent shift in gene expression. Therefore, these findings suggested that resistance to afatinib develops through a gradual, multi-phase alteration in gene expression.

Validation of afatinib resistance-associated gene signature and its prognostic relevance across patient cohorts. To validate the gene signatures associated with resistance to afatinib and assess their clinical relevance, RT-qPCR was performed on selected candidates. Several genes, including *BCAT1*, *GNG2*, *HSPA1A*, *ABLIM3*, *IL31RA*, *ROR1*, *SLCO2B1*, *HTR1D*, and *TBXAS1*, were consistently upregulated in the resistant cells compared with those in both the parental and afatinib-treated cells, consistent with the RNA-seq findings (Fig. 4A). HR analysis revealed that multiple genes, such as *ABLIM3*, *HTR1D* and *HSPA1A*, were significantly associated with both poor OS and DFS in clinical lung cancer datasets (Figs. 4B and C, S1 and S2). Furthermore, stage-specific expression analysis revealed the progressive upregulation of *ABLIM3*, *HTR1D* and *HSPA1A* from stage I to IV tumors, suggesting their involvement in tumor progression (Fig. 4D-F). The three-gene signature stratified patients into distinct risk groups, with individuals in the high-signature group demonstrating significantly shorter OS (HR=1.7; two-stage P<0.01) and DFS (HR=2.1; P<0.01) times (Fig. 4G and H). Notably, this signature retained prognostic significance for both OS and DFS across multiple cancer types, including liver, lung and pancreatic cancer (Figs. 4I and S3). Collectively, these findings identified *ABLIM3*, *HTR1D* and *HSPA1A* as an afatinib resistance-associated gene signature with prognostic value, underscoring their potential roles in tumor progression and patient risk stratification.

Pathway enrichment reveals MAPK/ERK signaling as a major contributor to resistance to afatinib. To elucidate the activated signaling pathways in adaptive response that also contribute to the stable resistance to afatinib, KEGG pathway enrichment analysis was conducted on upregulated genes from both the treated and resistant cells. In the treated cells, the 'MAPK signaling pathway' was identified as the most significantly enriched (P<0.01), whereas the resistant cells demonstrated an additional enrichment of the 'PI3K-AKT signaling pathway' (P<0.01), the 'Ras signaling pathway' (P<0.01) and 'TGF-β' (P<0.01) signaling (Fig. 5A and B), indicating the progressive and coordinated activation of pathways during resistance acquisition. To validate the activation of MAPK/ERK signaling in drug-treated and AR cells, the phosphorylation levels of ERK1/2 were examined using western blotting analysis. The results revealed that the p-ERK/ERK ratio was elevated by 1.7-fold in the treated A549 cells compared with that in the parental cells (P<0.05; Fig. 5C). Similarly, a 1.3-fold increase in the p-ERK/ERK ratio was observed in the AR cells (P<0.01; Fig. 5C), indicating the sustained activation of the MAPK/ERK pathway in the development of resistance to TKI. Furthermore, a correlation analysis demonstrated a significant positive correlation between the MAPK/ERK pathway activity and the expression levels of the three-gene signature (P<0.01; r=0.42; Fig. 5D). Collectively, these

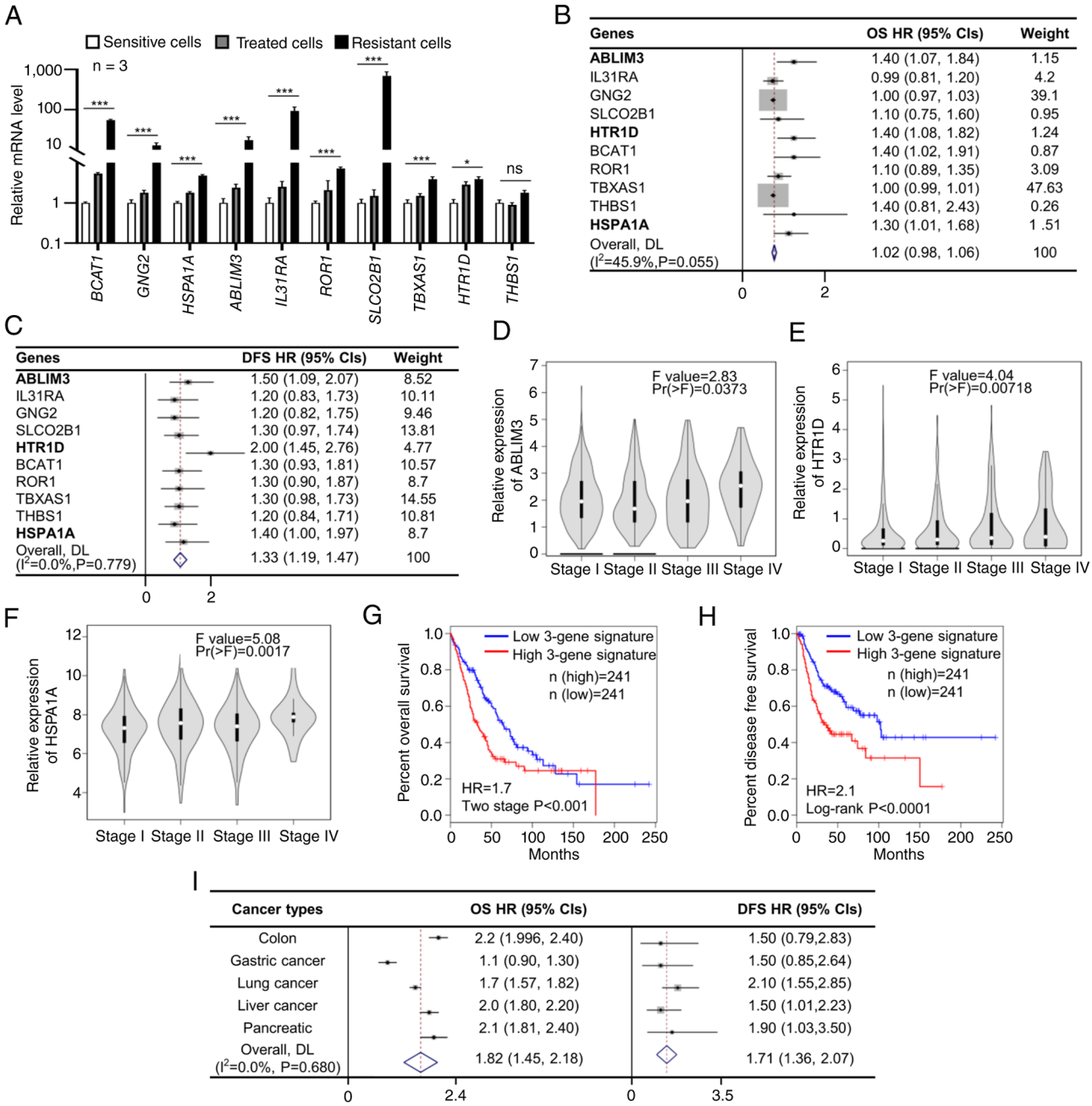

Figure 4. Validation of the afatinib resistance-associated gene signature and its prognostic relevance across patient cohorts. (A) Reverse transcription-quantitative PCR analysis of candidate gene expression in drug-sensitive (A549), treated A549, and resistant (A549-AR) cells (n=3). Statistical significance was assessed by one-way ANOVA followed by Dunnett's multiple-comparisons test versus the drug-sensitive group. (B and C) Forest plots summarizing HRs with 95% CIs for (B) OS and (C) DFS in patients with lung cancer with high expression versus low expression of the indicated genes. (D-F) Relative expression levels of (D) ABLIM3, (E) HTR1D and (F) HSPA1A in different stages of lung cancer. (G) OS and (H) DFS of patients with lung cancer with high expression of the 3-gene signature compared with those with low expression. For OS, Kaplan-Meier curves exhibiting crossover were compared over the full follow-up period using the two-stage procedure. For DFS, Kaplan-Meier curves were compared over the full follow-up period using the log-rank P-value. (I) OS and DFS of patients with various cancer types, comparing high versus low expression levels of ABLIM3, HTR1D and HSPA1A. *P<0.05; ***P<0.001. HTR1D, 5-hydroxytryptamine receptor 1D; ABLIM3, actin-binding LIM protein family member 3; HSPA1A, heat shock protein family A member 1A; OS, overall survival; DFS, disease-free survival; HR, hazard ratio; CI, confidence interval; DL, DerSimonian-Laird; Pr, probability; ns, not significant.

findings indicated that the MAPK/ERK signaling pathway was activated in the development of resistance to afatinib and was positively correlated with the identified three-gene signature. Due to previous reports implicating the role of TGF-β in TKI resistance across multiple malignancies, including lung and gastric cancer (22-24), TGF-β signaling was also selected for further investigation using specific inhibitors. To functionally assess the contribution of these pathways, A549-AR cells were treated with afatinib alone or in combination with either the TGF-β receptor inhibitor, SB431542 or the MEK inhibitor, selumetinib. Co-treatment with SB431542 led to no additional effect compared with afatinib alone, while co-treatment with 10 μM selumetinib significantly reduced the viability of resistant cells compared with afatinib treatment alone (P<0.01; Fig. 5E). These results demonstrated that MAPK/ERK signaling serves a functional role in mediating resistance to

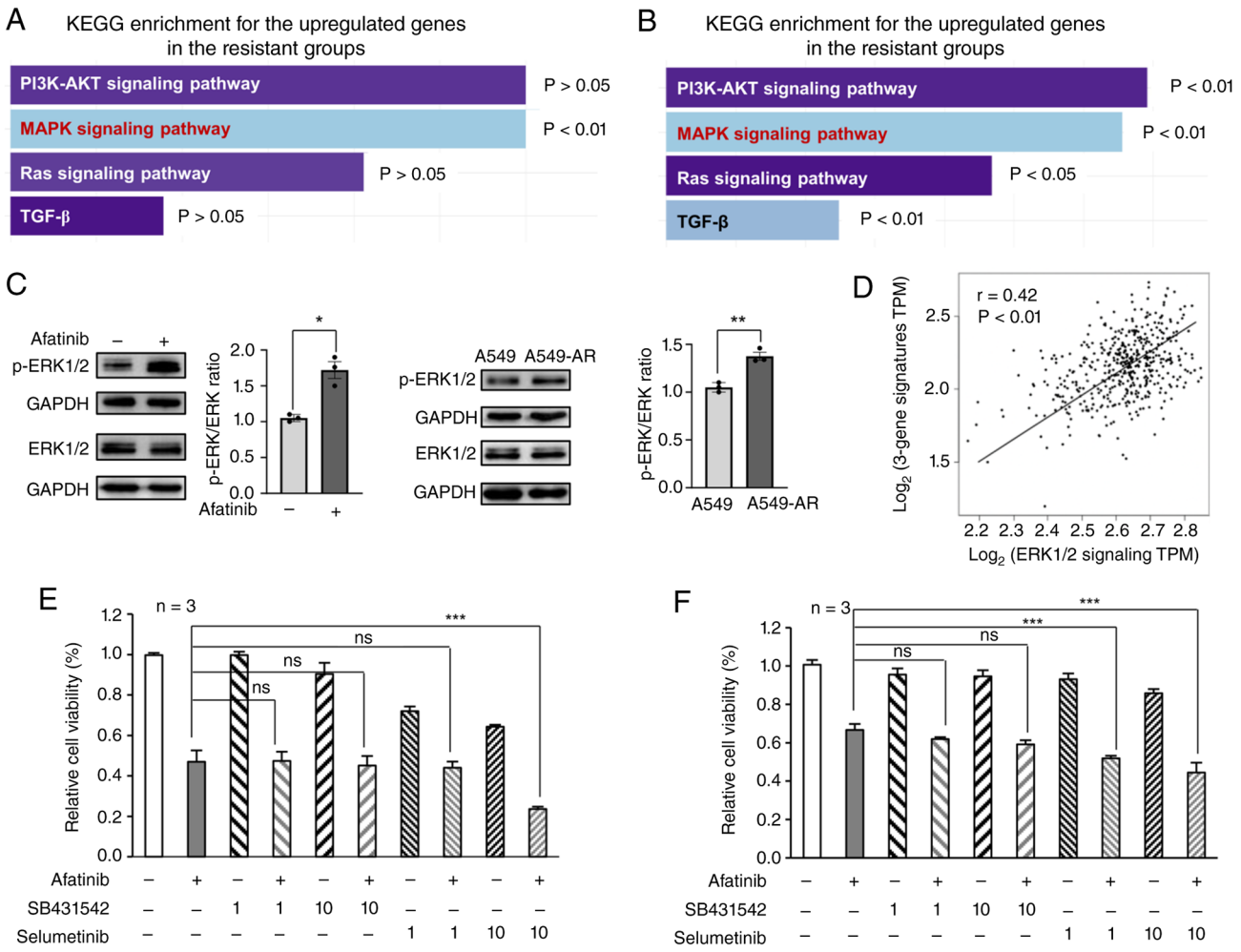

Figure 5. Pathway enrichment reveals MAPK/ERK signaling as a major contributor to resistance to afatinib. (A and B) KEGG enrichment of the upregulated genes in the (A) treated and (B) resistant groups. (C) Representative western blot images of ERK1/2 and p-ERK1/2, and quantification of the p-ERK/ERK ratio in A549 cells treated with 20 μM afatinib or in A549-AR cells. *P<0.05, **P<0.01, compared with the untreated group or A549 cells. (D) Correlation of the three-gene signature with ERK1/2 signaling in TCGA lung cancer data. (E) Relative cell viability of A549-AR cells treated with 10 μM afatinib in combination with either 1 or 10 μM SB431542 or selumetinib (n=3). Statistical significance was assessed by one-way ANOVA followed by Dunnett's multiple-comparisons test versus afatinib (10 μM). Adjusted P-values (Dunnett) are reported. (F) Relative cell viability of H1299-AR cells treated with 10 μM afatinib in combination with either 1 or 10 μM SB431542 or selumetinib (n=3). Statistical significance was assessed by one-way ANOVA followed by Dunnett's multiple-comparisons test versus the afatinib (10 μM) group. Adjusted P-values (Dunnett) are reported. ***P<0.001 and ns, no significance, compared with afatinib-treated group. AR, afatinib-resistant; p, phosphorylated; KEGG, Kyoto Encyclopedia of Genes and Genomes; TPM, transcript per million; TCGA, The Cancer Genome Atlas.

afatinib. Notably, the inhibition of MAPK/ERK signaling in H1299-AR cells restored sensitivity to afatinib, resulting in a >20% decrease in cell viability compared with afatinib monotherapy (P<0.01; Fig. 5F), further supporting its role as a major contributor to the resistant phenotype.

Inhibition of ERK signaling also reverses resistance to osimertinib. The aforementioned results showed that AR cells also exhibit resistance to osimertinib, suggesting that drug-induced adaptive responses may drive a broader, cross-resistant phenotype. Since the pharmacological inhibition of ERK signaling was sufficient to restore afatinib sensitivity, it was hypothesized that targeting this pathway may similarly reverse resistance to osimertinib. To validate this hypothesis, AR cells were treated with osimertinib in combination with either SB431542 or selumetinib. SB431542 alone had no inhibitory effect compared with the untreated control group and its combination with osimertinib did not enhance inhibition compared with osimertinib alone (Fig. 6A). By contrast, selumetinib monotherapy modestly reduced cell viability, while its combination with osimertinib produced a marked synergistic effect, resulting in an additional 20% reduction in viability compared with osimertinib treatment alone (P<0.01; Fig. 6A). Furthermore, selumetinib independently attenuated osimertinib resistance, as evidenced by a 10% greater suppression of cell viability compared with osimertinib monotherapy (P<0.01; Fig. 6B). These findings further support the role of sustained MAPK/ERK signaling in mediating cross-resistance and highlight the potential of targeted inhibition of ERK to restore sensitivity to EGFR-TKIs.

Discussion

The present study demonstrated that acquired resistance to afatinib also conferred cross-resistance to the third-generation EGFR inhibitor osimertinib, indicating that adaptive cellular

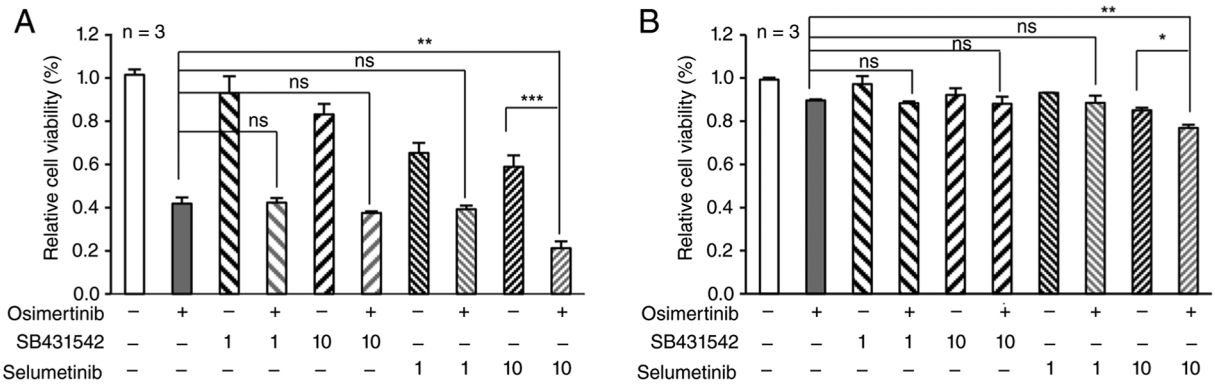

Figure 6. Inhibition of ERK signaling also reverses resistance to osimertinib. (A and B) Relative cell viability of (A) A549-AR and (B) H1299-AR cells treated with 10 μM osimertinib in combination with either 1 or 10 μM SB431542 or selumetinib (n=3). Statistical significance was assessed by one-way ANOVA followed by Tukey's multiple-comparisons test for comparisons between the osimertinib-alone group and the corresponding combination groups, and between 10 μM selumetinib alone and 10 μM selumetinib plus osimertinib. Adjusted P-values are reported. *P<0.05, **P<0.01 and ***P<0.001; ns, no significance. AR, afatinib-resistant.

responses, rather than secondary EGFR mutations, may serve a dominant role in the development of resistance. Mechanistically, resistance was associated with transcriptional reprogramming and the activation of the MAPK/ERK signaling pathway. A three-gene signature (*ABLIM3*, *HTR1D* and *HSPA1A*) was identified as a potential biomarker of resistance to afatinib and was positively correlated with MAPK/ERK pathway activity. Notably, the pharmacological inhibition of MAPK/ERK signaling using selumetinib effectively re-sensitized resistant cells to both afatinib and osimertinib. These findings highlighted MAPK/ERK pathway activation as a major contributor to resistance to EGFR-TKI and suggested that its targeted inhibition may represent a promising therapeutic strategy for NSCLC.

Since afatinib targets both wild-type and mutant EGFR, the present study employed EGFR-wild-type NSCLC models to specifically investigate EGFR-independent adaptive responses to TKI exposure. This approach minimizes the confounding effects of constitutively active EGFR mutations and enables a clearer characterization of stress-induced transcriptional programs that may precede or promote genetic resistance. By focusing on this model, the present study aimed to capture the early, non-mutational stage of resistance development, an adaptive process increasingly recognized as a major contributor to TKI treatment failure and a potential therapeutic target distinct from mutation-driven mechanisms.

Transcriptome analysis revealed that resistance of NSCLC cells to afatinib develops through a gradual transition from a drug-sensitive state to a stable resistant phenotype, beginning with an acute drug-induced stress response followed by persistent transcriptional reprogramming, consistent with previously reported heterogeneity in resistance mechanisms (16,25). The functional enrichment of resistance-associated gene clusters highlighted the aberrant regulation of kinase-phosphatase signaling, the upregulation of RNA metabolic activity, and the reorganization of cytoskeletal and adhesion structures, molecular features of cellular plasticity and therapeutic evasion. Among the oncogenic pathways, MAPK/ERK signaling emerged as a principal driver, with KEGG analysis indicating its early activation following exposure to afatinib. This activation was accompanied by the coordinated involvement of the PI3K/AKT, Ras and TGF-β pathways, which collectively contribute to the maintenance of the resistant phenotype (26-28). Notably, the modulation of the PI3K/AKT cascade has also been implicated in reversing the resistance of NSCLC cells to osimertinib, underscoring its interplay with MAPK/ERK signaling in acquired resistance to TKIs (29). Notably, pharmacological inhibition of ERK1/2 with selumetinib effectively reversed the resistance to both afatinib and osimertinib, supporting the key involvement of MAPK/ERK signaling in both the development and maintenance of acquired resistance to TKIs (30). These findings emphasize the complexity of dynamic, multi-pathway cooperation during resistance acquisition, suggesting that future therapeutic strategies may require the combined targeting of multiple signaling axes. Similar combined approaches, such as use of β-elemene in combination with hyperthermia, have been reported to enhance antitumor efficacy in NSCLC models (31), supporting the rationale for multi-target intervention.

The present study systematically investigated the role of the MAPK/ERK pathway in the development of resistance to EGFR-TKIs. It was demonstrated that the persistent activation of this pathway not only drives acquired resistance to the second-generation EGFR inhibitor, afatinib, but also mediates cross-resistance to the third-generation inhibitor, osimertinib, consistent with the findings of previous studies (32,33). Persistent ERK phosphorylation appears to promote stable signaling reprogramming independent of EGFR mutations, reflecting adaptive plasticity distinct from classical resistance mechanisms such as T790M or C797S mutations (34). This EGFR-independent resistance mode is consistent with previously reported bypass mechanisms involving the aberrant activation of signaling pathways, such as Src family kinase/focal adhesion kinase (35) or KRAS amplification (36).

Pharmacological validation confirmed the key role of MAPK/ERK signaling, as ERK inhibition restored the sensitivity to afatinib and osimertinib. These findings underscore MAPK/ERK activation as a central mediator of adaptive resistance. Furthermore, the present study identified a three-gene resistance signature (*ABLIM3*, *HTR1D* and *HSPA1A*), which was consistently upregulated in resistant cells and positively correlated with MAPK/ERK activity. Notably, HSPA1A can

enhance DUSP1 expression, a negative regulator of MAPK signaling (37), complementing previous research demonstrating that the loss of DUSP1 or DUSP6 leads to ERK activation and drug resistance (34). Therefore, these results delineate a mechanistic association between stress-induced transcriptional reprogramming and sustained ERK signaling in TKI-acquired resistance.

At a broader conceptual level, resistance to anticancer drugs is increasingly understood as an adaptive process within a complex pathological ecosystem rather than a phenomenon driven solely by genetic mutations (38). Tumor evolution involves dynamic interactions among cancer cells, stromal and immune components, and metabolic constraints that collectively shape therapeutic outcomes (39). From this ecological and evolutionary perspective, the transcriptional plasticity and signaling rewiring observed in AR cells likely reflect adaptive reprogramming under selective TKI pressure, maintaining the equilibrium between sensitive and resistant subpopulations (40,41). Integrating ecological and evolutionary principles with molecular insights may provide a more comprehensive understanding of acquired resistance and lead to the development of adaptive therapeutic strategies.

Notably, the *ABLIM3-HTR1D-HSPA1A* signature has demonstrated robust prognostic value across multiple solid tumors, including colorectal carcinoma (42), hepatocellular carcinoma (43) and pancreatic cancer, highlighting its potential as a pan-cancer biomarker for resistance-associated risk stratification. Compared with previously proposed single-gene markers such as neurotrophic tyrosine receptor kinase 2 (44) or AXL (45), this multi-gene signature provides greater predictive accuracy and broader clinical relevance. Building on these findings, the three-gene signature also holds translational potential as a clinically accessible biomarker. Among the three genes, HSPA1A, a member of the HSP70 family, is detectable in the circulation and is associated with tumor burden and treatment response (46,47). Although ABLIM3 has been detected at low abundance in plasma proteomic datasets (48) and HTR1D currently lacks circulating evidence, their co-expression patterns suggest possible applicability for liquid biopsy-based monitoring. Future studies are warranted to determine whether longitudinal changes in circulating or exosomal HSPA1A, ABLIM3 and HTR1D levels reflect emerging resistance or treatment response in patients with NSCLC receiving EGFR-TKIs. Validation in xenograft and patient-derived xenograft models with serial plasma sampling will be essential to confirm the *in vivo* detectability and prognostic relevance of this gene signature. Such efforts may enable the real-time, non-invasive tracking of adaptive resistance and accelerate the translation of these mechanistic insights into clinical practice.

Despite the comprehensive elucidation of the molecular mechanisms underlying the development of acquired resistance to afatinib in the present study, several limitations should be acknowledged. First, the findings presented herein are primarily based on *in vitro* models of NSCLC and lack *in vivo* validation using xenografts or patient-derived xenografts models. This limitation may affect the translational relevance of the results. Second, while the MAPK/ERK signaling pathway was identified as a major contributor to the resistant phenotype, the upstream regulatory mechanisms governing its activation remain incompletely understood. In particular, the involvement of alternative receptor tyrosine kinases, adaptor proteins or cellular stress-related pathways in sustaining ERK signaling requires further investigation. Furthermore, synergy metrics (for example, Chou-Talalay) were not included in the present study, as the primary objective was to delineate single-agent-induced adaptive responses. Future studies are thus warranted to incorporate systematic combination index analyses to quantitatively define synergistic or additive effects between EGFR-TKIs and MEK inhibitors. Lastly, the prognostic evaluation of *ABLIM3*, *HTR1D* and *HSPA1A* was based on transcriptomic datasets rather than clinical specimens. Thus, the future validation of their protein expression in NSCLC tissues using immunohistochemistry will be essential to confirm their prognostic significance and clinical applicability. In addition, Kaplan-Meier curves with crossover, particularly the DFS curve of HSPA1A and the OS curve of the three-gene signature in lung cancer, should be interpreted with caution. Although a two-stage analysis was additionally performed for these curves, it was based on reconstituted data derived from digitized Kaplan-Meier plots rather than original individual-level survival data.

Acknowledgements

The authors would like to thank Dr Ying Sun, a postdoctoral researcher at the School of Medicine, Shanghai Jiao Tong University (Shanghai, China), for providing help in operating RStudio.

Funding

The present study was funded by the National Natural Science Foundation of China (grant no. 82204673), the Budget Research Project of Shanghai University of Traditional Chinese Medicine (grant no. 2021LK018) and the Priority Incubation Program (grant no. A1-U24-205-030306).

Availability of data and materials

The data generated in the present study may be found in the Genome Sequence Archive in the National Genomics Data Center, China National Center for Bioinformation/Beijing Institute of Genomics, Chinese Academy of Sciences under accession number GSA-Human: HRA012241 or at the following URL: https://ngdc.cncb.ac.cn/gsa-human/browse/HRA012241. The remaining data generated in the present study may be requested from the corresponding author.

Authors' contributions

CQ participated in data acquisition, analysis and manuscript revision. WZ and DT conceived the study concept, and performed data interpretation and revision of the manuscript. YY and BL contributed to the acquisition of data and revised the manuscript. ZH and YZ contributed to the interpretation of data and revised the manuscript. TY conceived the study concept, drafted the manuscript and revised the manuscript.

WX conceived the study concept, contributed to data acquisition, analysis and interpretation, drafted the manuscript and revised the manuscript. All authors have read and approved the final manuscript. CQ and WX confirm the authenticity of all the raw data.

Ethics approval and consent to participate

Not applicable.

Patient consent for publication

Not applicable.

Competing interests

The authors declare that they have no competing interests.

References

1. Siegel RL, Giaquinto AN and Jemal A: Cancer statistics, 2024: CA Cancer J Clin 74: 12-49, 2024.
2. Xu L, Xu B, Wang J, Gao Y, He X, Xie T and Ye XY: Recent advances of novel fourth generation EGFR inhibitors in overcoming C797S mutation of lung cancer therapy. Eur J Med Chem 245: 114900, 2023.
3. Casal-Mouriño A, Ruano-Ravina A, Lorenzo-González M, Rodríguez-Martínez Á, Giraldo-Osorio A, Varela-Lema L, Pereiro-Brea T, Barros-Dios JM, Valdés-Cuadrado L and Pérez-Ríos M: Epidemiology of stage III lung cancer: Frequency, diagnostic characteristics, and survival. Transl Lung Cancer Res 10: 506-518, 2021.
4. Howlader N, Forjaz G, Mooradian MJ, Meza R, Kong CY, Cronin KA, Mariotto AB, Lowy DR and Feuer EJ: The effect of advances in lung-cancer treatment on population mortality. N Engl J Med 383: 640-649, 2020.
5. Riely GJ, Wood DE, Ettinger DS, Aisner DL, Akerley W, Bauman JR, Bharat A, Bruno DS, Chang JY, Chirieac LR, *et al*: Non-small cell lung cancer, version 4.2024, NCCN clinical practice guidelines in oncology. J Natl Compr Canc Netw 22: 249-274, 2024.
6. Liu Q, Yu S, Zhao W, Qin S, Chu Q and Wu K: EGFR-TKIs resistance via EGFR-independent signaling pathways. Mol Cancer 17: 53, 2018.
7. Sharma SV, Bell DW, Settleman J and Haber DA: Epidermal growth factor receptor mutations in lung cancer. Nat Rev Cancer 7: 169-181, 2007.
8. He J, Huang Z, Han L, Gong Y and Xie C: Mechanisms and management of 3rd-generation EGFR-TKI resistance in advanced non-small cell lung cancer (review). Int J Oncol 59: 90, 2021.
9. Kohsaka S, Nagano M, Ueno T, Suehara Y, Hayashi T, Shimada N, Takahashi K, Suzuki K, Takamochi K, Takahashi F and Mano H: A method of high-throughput functional evaluation of *EGFR* gene variants of unknown significance in cancer. Sci Transl Med 9: eaan6566, 2017.
10. Chen X, Zhu Q, Zhu L, Pei D, Liu Y, Yin Y, Schuler M and Shu Y: Clinical perspective of afatinib in non-small cell lung cancer. Lung Cancer 81: 155-161, 2013.
11. Ricciuti B, Metro G, Brambilla M, Ludovini V, Baglivo S, Siggillino A, Prosperi E and Chiari R: Acquired resistance to afatinib due to T790M-positive squamous progression in EGFR-mutant adenosquamous lung carcinoma. J Thorac Oncol 13: e9-e12, 2018.
12. Nakatani K, Yamaoka T, Ohba M, Fujita KI, Arata S, Kusumoto S, Taki-Takemoto I, Kamei D, Iwai S, Tsurutani J and Ohmori T: *KRAS* and *EGFR* amplifications mediate resistance to rociletinib and osimertinib in acquired afatinib-resistant NSCLC harboring exon 19 deletion/T790M in *EGFR*. Mol Cancer Ther 18: 112-126, 2019.
13. Torigoe H, Shien K, Takeda T, Yoshioka T, Namba K, Sato H, Suzawa K, Yamamoto H, Soh J, Sakaguchi M, *et al*: Therapeutic strategies for afatinib-resistant lung cancer harboring HER2 alterations. Cancer Sci 109: 1493-1502, 2018.
14. Nishimura J, Miyamoto Y, Fujimoto N, Ozeki T, Takada K, Asano M, Fuchimoto Y, Wada S, Ozaki S and Kishimoto T: Adenocarcinoma of the lung acquiring resistance to afatinib by transformation to small cell carcinoma: A case report. Case Rep Oncol 10: 666-670, 2017.
15. Nakamura T, Nakashima C, Komiya K, Kitera K, Hirai M, Kimura S and Aragane N: Mechanisms of acquired resistance to afatinib clarified with liquid biopsy. PLoS One 13: e0209384, 2018.
16. Zhu X, Zhou R, Lu Y, Zhang Y, Chen Q and Li Y: Identification and validation of afatinib potential drug resistance gene *BIRC5* in non-small cell lung cancer. Front Oncol 11: 763035, 2021.
17. Cremers CG and Nguyen LK: Network rewiring, adaptive resistance and combating strategies in breast cancer. Cancer Drug Resist 2: 1106-1126, 2019.
18. Kumar U, Castellanos-Uribe M, May ST and Yagüe E: Adaptive resistance is not responsible for long-term drug resistance in a cellular model of triple negative breast cancer. Gene 850: 146930, 2023.
19. Gevertz JL, Greene JM, Prosperi S, Comandante-Lou N and Sontag ED: Understanding therapeutic tolerance through a mathematical model of drug-induced resistance. NPJ Syst Biol Appl 11: 30, 2025.
20. Chatterjee N and Bivona TG: Polytherapy and targeted cancer drug resistance. Trends Cancer 5: 170-182, 2019.
21. Livak KJ and Schmittgen TD: Analysis of relative gene expression data using real-time quantitative PCR and the 2(-delta delta C(T)) method. Methods 25: 402-408, 2001.
22. Fan W, Xing Y, Yan S, Liu W, Ning J, Tian F, Wang X, Zhan Y, Luo L, Cao M, *et al*: DUSP5 regulated by YTHDF1-mediated m6A modification promotes epithelial-mesenchymal transition and EGFR-TKI resistance via the TGF-β/Smad signaling pathway in lung adenocarcinoma. Cancer Cell Int 24: 208, 2024.
23. Chen J, Hai Y, Hu Q, Chen C, Jiang X and Gao Y: TGF-β signaling activation confers anlotinib resistance in gastric cancer. Pharm Res 40: 689-699, 2023.
24. Shen H, Guan D, Shen J, Wang M, Chen X, Xu T, Liu L and Shu Y: TGF-β1 induces erlotinib resistance in non-small cell lung cancer by down-regulating PTEN. Biomed Pharmacother 77: 1-6, 2016.
25. Yamaoka T, Ohmori T, Ohba M, Arata S, Murata Y, Kusumoto S, Ando K, Ishida H, Ohnishi T and Sasaki Y: Distinct afatinib resistance mechanisms identified in lung adenocarcinoma harboring an EGFR mutation. Mol Cancer Res 15: 915-928, 2017.
26. Zhang J, Sun B, Ruan X, Hou X, Zhi J, Meng X, Zheng X and Gao M: Oncoprotein HBXIP promotes tumorigenesis through MAPK/ERK pathway activation in non-small cell lung cancer. Cancer Biol Med 18: 105-119, 2021.
27. Hijazi M, Casado P, Akhtar N, Alvarez-Teijeiro S, Rajeeve V and Cutillas PR: eEF2K activity determines synergy to cotreatment of cancer cells with PI3K and MEK inhibitors. Mol Cell Proteomics 21: 100240, 2022.
28. Zhang Z, Richmond A and Yan C: Immunomodulatory properties of PI3K/AKT/mTOR and MAPK/MEK/ERK inhibition augment response to immune checkpoint blockade in melanoma and triple-negative breast cancer. Int J Mol Sci 23: 7353, 2022.
29. Lai L, Shen Q, Wang Y, Chen L, Lai J, Wu Z and Jiang H: Polyphyllin I reverses the resistance of osimertinib in non-small cell lung cancer cell through regulation of PI3K/Akt signaling. Toxicol Appl Pharmacol 419: 115518, 2021.
30. Munck JM, Berdini V, Bevan L, Brothwood JL, Castro J, Courtin A, East C, Ferraldeschi R, Heightman TD, Hindley CJ, *et al*: ASTX029, a novel dual-mechanism ERK inhibitor, modulates both the phosphorylation and catalytic activity of ERK. Mol Cancer Ther 20: 1757-1768, 2021.
31. Wu Z, Wang T, Zhang Y, Zheng Z, Yu S, Jing S, Chen S, Jiang H and Ma S: Anticancer effects of β-elemene with hyperthermia in lung cancer cells. Exp Ther Med 13: 3153-3157, 2017.
32. Liu Z, Chen Z, Wang J, Zhang M, Li Z, Wang S, Dong B, Zhang C, Gao J and Shen L: Mouse avatar models of esophageal squamous cell carcinoma proved the potential for EGFR-TKI afatinib and uncovered Src family kinases involved in acquired resistance. J Hematol Oncol 11: 109, 2018.
33. Li Y, Zang H, Qian G, Owonikoko TK, Ramalingam SR and Sun SY: ERK inhibition effectively overcomes acquired resistance of epidermal growth factor receptor-mutant non-small cell lung cancer cells to osimertinib. Cancer 126: 1339-1350, 2020.

34. He W, Liu P, Lei Q, Xu J and Liu L: DUSP1 promotes osimertinib drug-tolerant persistence by inhibiting MAPK/ERK signaling in non-small cell lung cancer. Mol Biotechnol 67: 1256-1268, 2025.
35. Ichihara E, Westover D, Meador CB, Yan Y, Bauer JA, Lu P, Ye F, Kulick A, de Stanchina E, McEwen R, *et al*: SFK/FAK signaling attenuates osimertinib efficacy in both drug-sensitive and drug-resistant models of EGFR-mutant lung cancer. Cancer Res 77: 2990-3000, 2017.
36. Lee TG, Kang HM, Kim SY, Kim HR and Kim CH: The combination of osimertinib with Raf inhibitor overcomes osimertinib resistance induced by KRAS amplification in EGFR-mutated lung cancer cells. Exp Cell Res 430: 113722, 2023.
37. He X, Deng B, Zhang C, Zhang G, Yang F, Zhu D, Yang Y, Ma B, Hu X, Wang Y and Kang X: HSPA1A inhibits pyroptosis and neuroinflammation after spinal cord injury via DUSP1 inhibition of the MAPK signaling pathway. Mol Med 31: 53, 2025.
38. Nie C, Qi Y, Wang T, Shan Y, Xie C, Jiang Z, Ke Z, Zhang L, Du S, Xiong H and Yao J: Nanodrug-based therapeutic interventions for tumor-associated microbiota modulation. J Control Release 387: 114196, 2025.
39. Beyaert SP, Loriot AE, Huyghe ND, Goebbels RM, Mendola A, Govaerts AS, Fortpied C, Baldin P, Licitra LF, Lalami Y, *et al*: Tumor microenvironment modifications induced by afatinib in squamous cell carcinoma of the head and neck: A window-of-opportunity study (EORTC-90111-24111). Clin Cancer Res 29: 4076-4087, 2023.
40. Luo WR: Rethinking cancer: Zhonghua Zhong Liu Za Zhi 47: 463-467, 2025 (In Chinese).
41. Luo W: Nasopharyngeal carcinoma ecology theory: Cancer as multidimensional spatiotemporal 'unity of ecology and evolution' pathological ecosystem. Theranostics 13: 1607-1631, 2023.
42. Zhang H, Liu J, Dang Q, Wang X, Chen J, Lin X, Yang N, Du J, Shi H, Liu Y and Han J: Ribosomal protein RPL5 regulates colon cancer cell proliferation and migration through MAPK/ERK signaling pathway. BMC Mol Cell Biol 23: 48, 2022.
43. Sun Y, Lan M, Chen X, Dai Y, Zhao X, Wang L, Zhao T, Li Y, Zhu J, Zhang X, *et al*: Anti-invasion and anti-metastasis effects of Valjatrate E via reduction of matrix metalloproteinases expression and suppression of MAPK/ERK signaling pathway. Biomed Pharmacother 104: 817-824, 2018.
44. Wang Y, Liu C, Chen H, Jiao X, Wang Y, Cao Y, Li J, Zhang X, Sun Y, Zhuo N, *et al*: Clinical efficacy and identification of factors confer resistance to afatinib (tyrosine kinase inhibitor) in EGFR-overexpressing esophageal squamous cell carcinoma. Signal Transduct Target Ther 9: 153, 2024.
45. Murakami Y, Kusakabe D, Watari K, Kawahara A, Azuma K, Akiba J, Taniguchi M, Kuwano M and Ono M: AXL/CDCP1/SRC axis confers acquired resistance to osimertinib in lung cancer. Sci Rep 12: 8983, 2022.
46. Chanteloup G, Cordonnier M, Isambert N, Bertaut A, Hervieu A, Hennequin A, Luu M, Zanetta S, Coudert B, Bengrine L, *et al*: Monitoring HSP70 exosomes in cancer patients' follow up: A clinical prospective pilot study. J Extracell Vesicles 9: 1766192, 2020.
47. Werner C, Stangl S, Salvermoser L, Schwab M, Shevtsov M, Xanthopoulos A, Wang F, Dezfouli AB, Thölke D, Ostheimer C, *et al*: Hsp70 in liquid biopsies-a tumor-specific biomarker for detection and response monitoring in cancer. Cancers (Basel) 13: 3706, 2021.
48. Qu Y, Yao Z, Xu N, Shi G, Su J, Ye S, Chang K, Li K, Wang Y, Tan S, *et al*: Plasma proteomic profiling discovers molecular features associated with upper tract urothelial carcinoma. Cell Rep Med 4: 101166, 2023.